# Tapering photonic crystal fibers for generating self-similar ultrashort pulses at 1550 nm

Annamalai Manimegalai
Krishnamoorthy Senthilnathan
Kaliyaperumal Nakkeeran
Padmanabhan Ramesh Babu

**SPIE.**

# Tapering photonic crystal fibers for generating self-similar ultrashort pulses at 1550 nm

Annamalai Manimegalai,[a] Krishnamoorthy Senthilnathan,[b] Kaliyaperumal Nakkeeran,[c] and
Padmanabhan Ramesh Babu[b],*
[a]VIT University, School of Electronics Engineering, Vellore, Tamil Nadu 632014, India
[b]VIT University, Department of Physics, School of Advanced Sciences, Vellore, Tamil Nadu 632014, India
[c]University of Aberdeen, School of Engineering, Fraser Noble Building, Kings College, Aberdeen AB24 3UE, United Kingdom

**Abstract.** The generation of high-quality self-similar ultrashort pulses at 1550 nm by tapering the photonic crystal fibers (PCFs) is numerically demonstrated. We taper the PCF to achieve the exponentially decreasing dispersion and exponentially increasing nonlinearity profiles, which turn out to be the fundamental requirements for generating the chirped self-similar pulses. Further, we find that the chirped solitons could also be generated with the other three possible exponential variations. Thus, for the first time, we attempt tapering the PCFs for bringing in these exponentially varying dispersion and nonlinear profiles. We carry out the detailed pulse compression studies for various decay rates of the dispersion profiles as the decay rates of dispersion depend on the initial chirp and hence on compression factor, too. The unique feature of this pulse compressor lies in the fact that the required length of the tapered PCF is about 20 times less than that of the previously reported pulse compressor operating at 850 nm. © 2016 Society of Photo-Optical Instrumentation Engineers (SPIE) [DOI: 10.1117/1.OE.55.6.067108]

## 1 Introduction

In recent times, ultrashort pulses (USPs) have received much attention owing to their applications in various areas such as optical sampling systems, infrared time-resolved spectroscopy, ultrafast physical processes, and ultrahigh-bit-rate optical communication systems.[1–3] Although several techniques are being used for generating USPs, pulse compression technique is preferred for several reasons.[4] Pulse compression in fiber was first investigated by Mollenauer et al.[5] In general, pulse compression in optical media is classified into two types: linear compression and nonlinear compression. Using a dispersive fiber delay line or grating pairs, linear compression of chirped pulses has been demonstrated.[1,6] Recently, three nonlinear pulse compression techniques, adiabatic pulse compression, higher order soliton pulse compression, and self-similar techniques, have been developed. Generally, nonlinear pulse compression depends on the interplay between the self-phase modulation and group-velocity dispersion (GVD).[1] It is known that the adiabatic pulse compression demands lengthy fibers as the dispersion varies slowly.[7] However, in the higher order soliton pulse compression technique, the compressed pulses do suffer from significant pedestal generation, which eventually results in nonlinear interactions between neighboring solitons.[8]

For the first time, Moores[9] has investigated the generation of exact chirped soliton in an exponentially varying dispersive medium by solving the variable nonlinear Schrodinger (NLS) equation. More recently, linearly chirped solitary type pulses have been investigated in both optical fibers and fiber Bragg grating using self-similar analysis.[10,11] This new compression technique facilitates rapid pulse compression

without the stringent requirement of the adiabatic pulse compression, and hence, it provides efficient pulse compression. From the literature survey, it may be inferred that tapering the conventional optical fibers has been a challenging task due to the practical limitations.[12] However, very recently, a fiber called photonic crystal fiber (PCF) has been proposed. Owing to the feasibility of altering the fiber parameters, one could easily control the dispersion and nonlinear properties along the propagation direction.[13,14]

The flame brushing technique is a common method for fabricating the fiber that is discussed in this work. Initially, the required number of capillaries was made to form a periodic hexagonal preform with two rings, air holes arranged around a core using stack and draw technique.[15] This preform was covered and pulled in a fiber drawing tower to form PCF. Then, the tapering can be done by a promising fabrication technique called flame brushing technique.[16] In this technique, the fiber is heated with uniform temperature, and then tapering is made by consequently stretching the heated fiber. When tapering the PCF, the surface tension causes lessening of the air holes as the fiber gets heated. As a result, the diameter of the air hole decreases and the effective area increases. The different shapes of the tapers can be made by fiber perturbations.[17] Especially, the exponential tapering could be done by predicting exact hot zone length and taper expansion.[18]

Very recently, self-similar pulse compression at 850 nm was numerically demonstrated in a tapered PCF (TPCF) with exponentially decreasing dispersion and exponentially increasing nonlinearity.[19] In addition, the possibility of generating a train of USPs at near-infrared regime in a TPCF using raised-cosine pulses was also numerically demonstrated.[20]

*Address all correspondence to: Padmanabhan Ramesh Babu, E-mail: prameshbabu@vit.ac.in

Highly coherent supercontinuum generation with picosecond pulses by using self-similar compression using tapered fiber has also been demonstrated.[21] Recently, the effective pulse compression has been studied in linearly decreasing dispersion and nonlinearity increasing fibers with constant dispersion and increasing nonlinearity.[22] In this paper, we intend to investigate the possibility of compressing the chirped self-similar solitary type pulses at 1550 nm in exponentially decreasing dispersion and exponentially increasing nonlinearity. The 1550-nm wavelength is chosen because of the low-absorption characteristics of the silica material used in fibers. With the self-similar conditions, one can have four different possibilities of designing TPCFs that rely on engineering the dispersion and nonlinearity, which may be suitable for several applications. To the best of our knowledge, only one possibility of designing TPCF through self-similar conditions has been exploited for generating USPs and for supercontinuum generation. In this paper, we also address the all four possibilities of designing the TPCF through self-similar conditions.

The paper is organized as follows. Section 2 presents the theoretical modeling of the proposed work. We explore all possibilities of generating USPs through self-similar conditions in Sec. 3. We explore the designs of four TPCFs by implementing finite element method (FEM) in Sec. 4. We deal with the pulse compression studies through self-similar analysis in Sec. 5. We delineate the importance of initial chirp for getting efficient pulse compression and choosing the optimal initial value through different decay factors in Sec. 6. Finally, we conclude the research findings in Sec. 7.

## 2 Theoretical Model

The light pulse propagation in a TPCF is governed by the following well-known modified NLS equation[9]

$$\frac{\partial U}{\partial z} + i\frac{\beta_2(z)}{2}\frac{\partial^2 U}{\partial t^2} - i\gamma(z)|U|^2 U + \frac{g(z)}{2}U = 0, \tag{1}$$

where $U$ is the slowly varying envelope of the wave, $z$ is the longitudinal coordinate, and $t$ is the time in the moving reference frame. The parameters $\beta_2(z)$, $\gamma(z)$, and $g(z)$ are the varying second-order dispersion coefficient, varying nonlinear coefficient, and the distributed gain/loss, respectively. We assume that the self-similar solution of Eq. (1) is[20,23]

$$U(z, t) = \frac{1}{\sqrt{1 - \alpha_{20}D(z)}} R\left[\frac{t - T_c}{1 - \alpha_{20}D(z)}\right]$$
$$\times \exp\left[i\alpha_1(z) + i\frac{\alpha_2(z)}{2}(t - T_c)^2\right]\exp[G(z)/2], \tag{2}$$

where $T_c$, $D(z)$, $\alpha_{20}$, and $G(z)$ are the center of the pulse, the cumulative dispersion, initial chirp value, and cumulative gain/loss, respectively. $R$ defines a function with the parameters of $t$, $T_c$, $\alpha_{20}$, and $D(z)$. The parameters $\alpha_1$ and $\alpha_2$ are the constant phase and chirp, respectively. The chirped pulses demand the following necessary and sufficient condition connected to dispersion, nonlinearity, and gain of the medium. Finally, the chirped bright solitary wave in a TPCF is given by[19,20]

$$U(z, t) = \sqrt{\frac{|\beta_{20}|e^{(-\sigma z)}}{\gamma_0 e^{\rho z}}} \frac{1}{T_0 e^{-\sigma z}} \text{sech}\left[\frac{t - T_c}{T_0 e^{-\sigma z}}\right]$$
$$\times \exp\left[i\alpha_{10} + i\frac{\beta_{20}}{2\sigma T_0^2} \times (1 - \exp^{\sigma z}) + i\frac{\sigma \exp^{\sigma z}}{2\beta_{20}}(t - T_c)^2\right]. \tag{3}$$

In contrast to the conventional soliton, the above solitary pulse possesses the linear chirp. This chirped solitary pulse implies two-stage dynamics of pulse evolution. That is, initially, linear effect overwhelms the nonlinearity, which, in turn, plays a minor role, and hence, this process facilitates quasilinear pulse compression. On the other hand, in the final stage, the nonlinear effect dominates the linear effect. Consequently, one achieves the nonlinear compression. In addition, from the above chirped soliton solution, it is very clear that the intensity and chirp increase exponentially and the width decreases exponentially.

At this juncture, from Eq. (1), we recall that there is a physical constraint that does not allow the three distributed parameters to vary along the propagation direction simultaneously. However, it does allow any two of them to vary simultaneously by keeping a third one constant. Therefore, to realize a most physically valid system, we consider variation of dispersion and the nonlinearity by assuming a constant loss. Accordingly, we have

$$\beta_2(z) = \beta_{20} \exp(-\sigma z), \tag{4}$$

$$\gamma(z) = \gamma_0 \exp(\rho z), \tag{5}$$

where $\beta_{20}$, $\sigma$ ($=2\alpha_{20}\beta_{20}$), $\gamma_0$, and $\rho$ are the initial dispersion, dispersion decay rate, initial nonlinearity, and nonlinear growth rate, respectively. We substitute the dispersion and nonlinearity varying parameters in Eq. (3) to prove that loss is a constant one. With these conditions, we obtain following expression for $g(z)$:

$$g(z) = -\rho - \frac{-\sigma(\nu - 1)}{\nu - 1 + \exp(-\sigma z)}, \tag{6}$$

where

$$\nu = \frac{\sigma}{\alpha_{20}\beta_{20}}. \tag{7}$$

The loss/gain profile becomes a constant only when $\nu = 1$. From the above discussion, we infer that the chirped solitons could exist if and only if the dispersion decreases exponentially and the nonlinearity increases exponentially with loss being a constant.

## 3 Sustaining Self-Similar Pulses for Possible Conditions

In this section, we explore the other possibilities of generating the chirped solitons for various choices of positive and negative exponentially varying dispersion and nonlinearity, which are listed below.

1. GVD decreases and nonlinearity increases

$$\beta_2(z) = \beta_{20} \exp(-\sigma z), \quad \gamma(z) = \gamma_0 \exp(\rho z). \quad (8)$$

2. Both GVD and nonlinearity decrease

$$\beta_2(z) = \beta_{20} \exp(-\sigma z), \quad \gamma(z) = \gamma_0 \exp(-\rho z). \quad (9)$$

3. GVD increases and nonlinearity decreases

$$\beta_2(z) = \beta_{20} \exp(\sigma z), \quad \gamma(z) = \gamma_0 \exp(-\rho z). \quad (10)$$

4. Both GVD and nonlinearity increase

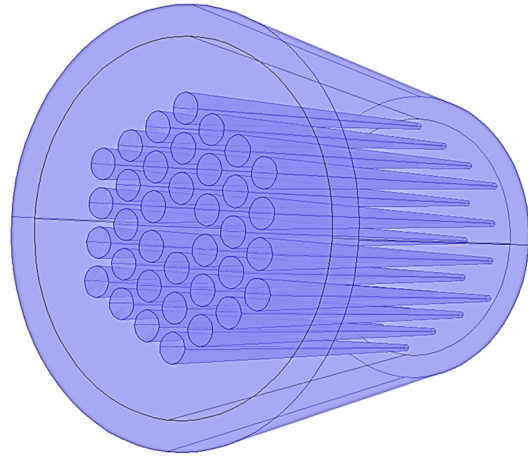$$\beta_2(z) = \beta_{20} \exp(\sigma z), \quad \gamma(z) = \gamma_0 \exp(\rho z). \quad (11)$$



**Fig. 1** 3-D picture of the proposed single-mode TPCF.

These physically valid conditions are not merely mathematical conditions for the existence of chirped soltions. Rather each of these conditions represents the different medium. That is, one gets four distinct PCFs that satisfy their corresponding mathematical conditions.

## 4 Designing of Tapered Photonic Crystal Fibers Through Self-Similar Conditions

The next step is to explore the various designs of PCFs by appropriately varying the design parameters, namely, pitch and relative air-hole diameter. We identify that the pitch and the diameter of air holes must vary exponentially to meet the above-mentioned conditions on tapering the PCFs. The GVD and nonlinearity values are numerically calculated by FEM.[24] In what follows, we delineate the four designs of PCFs.

### 4.1 Group-Velocity Dispersion Decreases and Nonlinearity Increases

When the fiber is tapered, the core diameter decreases along the propagation direction. Upon the fiber being tapered, the mode confinement is increasing. This means that the dispersion decreases exponentially all along. On the other hand, effective mode area decreases due to tapering. As a result, the nonlinearity increases exponentially. We note that the generation of self-similar USPs at 850 nm has been studied in a TPCF of exponentially decreasing dispersion and exponentially increasing profiles.[19] In addition, an attempt has also been made to generate a train of USPs at 850 nm using raised-cosine pulses.[20] Recently, TPCF has been fabricated to get dispersion decreasing and nonlinearity increasing profiles.[25]

As a first step, based on the analytical results of Eq. (8), we design the PCF at 1550 nm to meet exponentially decreasing dispersion and exponentially increasing nonlinearity profiles. While tapering the PCF, we decrease the diameter of air holes and the pitches exponentially. To study the self-similar pulse compression at 1550 nm, we design the PCF to get a maximum possible dispersion, which helps realize a compact compressor as the corresponding dispersion length $L_D (= T_0^2/\beta_2)$ becomes less. Figure 1 shows the three-dimensional (3-D) picture of the proposed PCF. Figure 2 shows the mode-field distribution of the proposed silica core TPCF. We calculate the initial GVD as −95.97 ps²/km by
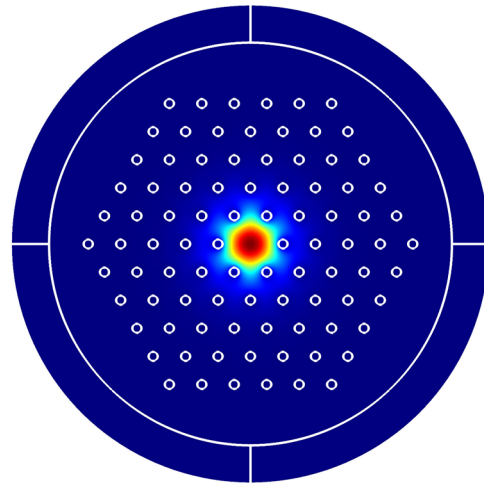


**Fig. 2** Mode-field distribution of the proposed single-mode TPCF of silica core with $d/\Lambda = 0.2796$ and pitch = 4 $\mu$m.

deploying FEM for the PCF parameters of $d/\Lambda = 0.2796$ and $\Lambda = 4$ $\mu$m. We choose the PCF of length $L = 4.29$ m, which is two times the dispersion length ($L = 2L_D$), where $L_D = 2.156$ m for a given pulse width of 0.8 ps. Here, we vary the relative air-hole diameter $d/\Lambda$ from 0.2796 to 0.2910 and the $\Lambda$ from 4 to 3.5 $\mu$m. Figure 3(a) shows the variation of design parameters, namely, relative air-hole diameter and pitch, against propagation distance $z$. The variations of computed optical properties, namely, GVD and nonlinearity, with respect to the distance are shown in Fig. 3(b). The cumulative dispersion $\beta_2$ at the end of the PCF is found to be −7.52 ps²/km. We next calculate the effective nonlinearity by using effective mode area $A_{\text{eff}}$. The initial and final values of $A_{\text{eff}}$ are found to be 40.72 and 35.83 $\mu$m², respectively. The initial nonlinearity is 2.587 W⁻¹ km⁻¹. By taking into account $A_{\text{eff}}$ for four different PCF structures, the effective nonlinearity of the tapered fiber is estimated by using the relation $\gamma = (2\pi n_2/\lambda A_{\text{eff}})$, where $n_2$ value is $2.6 \times 10^{-20}$ m²/W. The decrease in effective area leads to significant increases in intensity of the pulses.

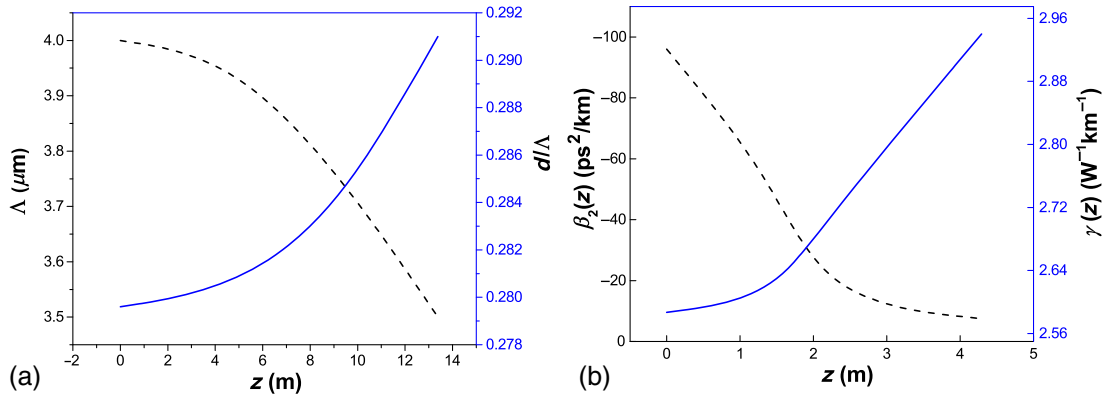**Fig. 3** (a) Variation of PCF design parameters $\Lambda$ and $d/\Lambda$ along the propagation distance $z$ and (b) variation of GVD $\beta_2(z)$ and nonlinearity $\gamma(z)$ as a function of propagation distance $z$.

### 4.2 Both Group-Velocity Dispersion and Nonlinearity Decrease

Now, we design the PCF to get both decreasing dispersion and nonlinearity to satisfy the physical conditions of Eq. (9). In this case, we decrease the diameter of the air holes and keep the pitch as a constant. We choose the PCF of length $L = 8$ m, which is four times the dispersion length ($L = 4L_D$), where $L_D = 2.02$ m. Here, the relative air-hole diameters vary exponentially from 0.2530 to 0.2346, the diameters of the air holes vary from 0.62 to 0.575 $\mu$m and the pitch is fixed as 2.45 $\mu$m. Figures 4(a) and 4(b) show the variations of design parameters and calculated optical properties against the propagation distance.

### 4.3 Group-Velocity Dispersion Increases and Nonlinearity Decreases

In this case, we focus on designing the PCF for increasing GVD and decreasing nonlinearity profiles. We obtain the required profiles by arbitrarily varying the relative air-hole diameter and pitch. While tapering the PCF, we decrease the diameter of the air holes and keep the pitch as a constant. We choose the PCF of length $L = 1.493$ km, which is four times the dispersion length ($L = 4L_D$), where $L_D = 373.413$ m. Here, the relative air-hole diameters vary exponentially from 0.3 to 0.2804, the air-hole diameters vary from 1.141 to 0.953 $\mu$m, and the pitch varies from 3.804 to

4 $\mu$m. Figures 5(a) and 5(b) show the variations of design parameters and calculated optical properties with respect to propagation distance. Very recently, the pulse compression has been demonstrated experimentally in dispersion increasing and constant nonlinearity optical medium.[26]

### 4.4 Both Group-Velocity Dispersion and Nonlinearity Increase

The last case deals with designing PCF for both increasing dispersion and nonlinearity profiles, which are obtained by arbitrarily varying the design parameters by keeping the pitch as a constant. We choose the PCF of length $L = 186.980$ m, which is four times the dispersion length ($L = 4L_D$), where $L_D = 46.745$ m. Here, we vary the relative air-hole diameters from 0.2653 to 0.2838 and the pitch from 2.45 to 2.29 $\mu$m with the air-hole diameter being 2.45 $\mu$m. The variations of design parameters and linear and nonlinear properties against the propagation distance are shown in Figs. 6(a) and 6(b), respectively. In Ref. 27, the tunable spectral compression has been studied numerically and experimentally in dispersion increasing and constant nonlinearity fiber medium.

Thus, one could carry out the self-similar pulse compression studies by using the various hitherto designed PCFs. From the literature survey, it is very clear that the soliton-based pulse compression has been studied widely in dispersion decreasing nonlinear media. However, though there are
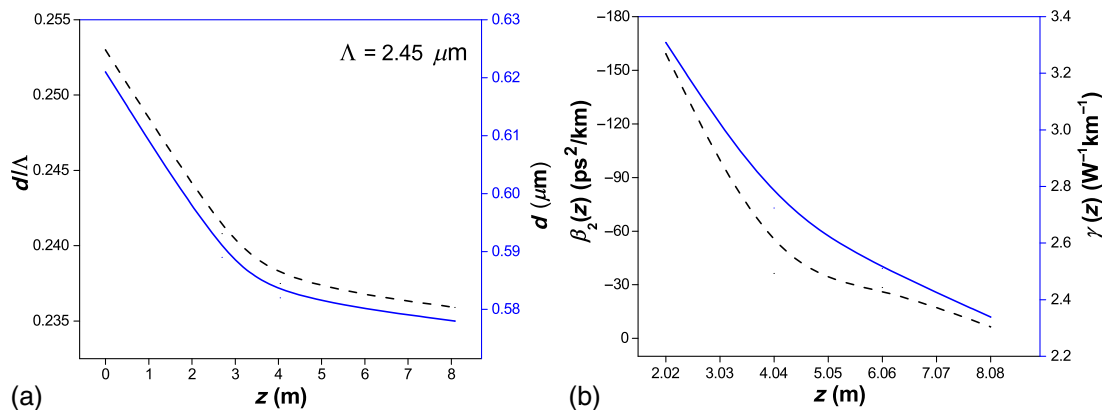


**Fig. 4** (a) Variation of PCF design parameters $d/\Lambda$ and $d$ along the propagation distance $z$ and (b) variation of GVD $\beta_2(z)$ and nonlinearity $\gamma(z)$, as a function of propagation distance $z$.
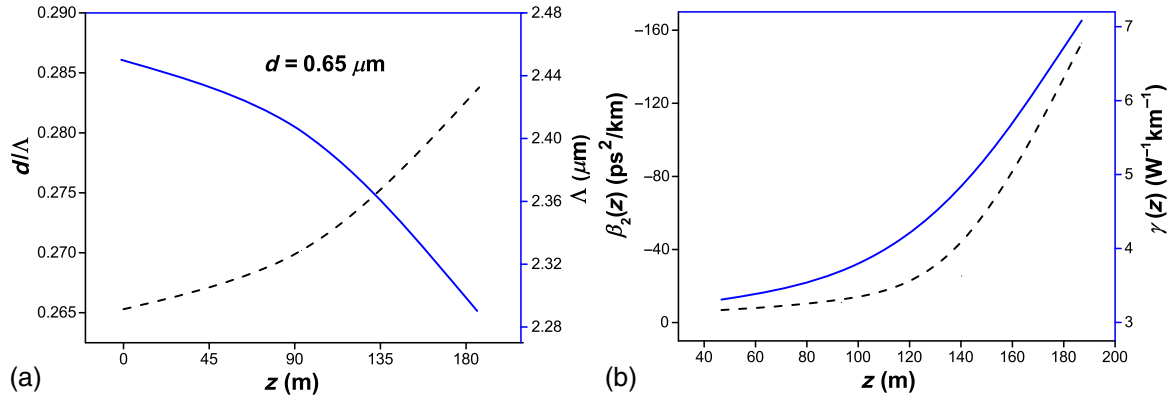
**Fig. 5** (a) Variation of PCF design parameters $d/\Lambda$ and $\Lambda$ along the propagation distance $z$ and (b) variation of GVD $\beta_2(z)$ and nonlinearity $\gamma(z)$ as a function of propagation distance $z$ in accordance with Eq. 10.
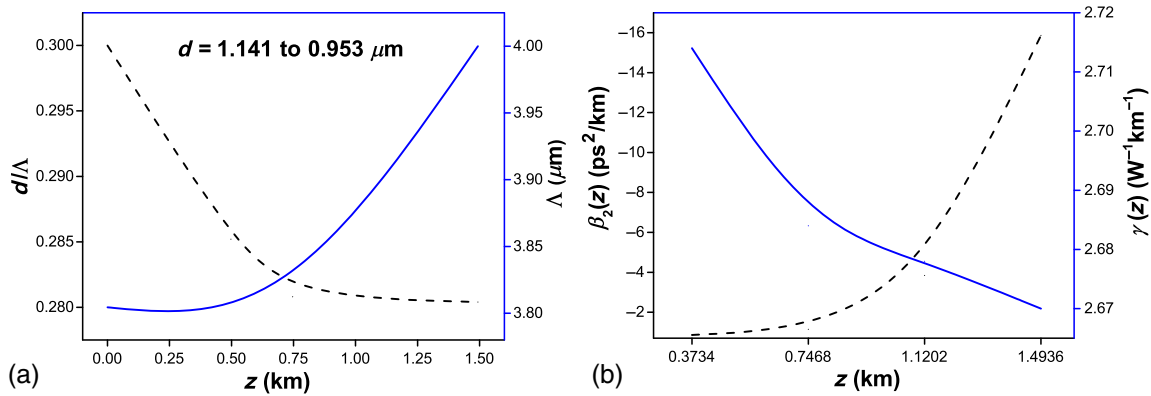


**Fig. 6** (a) Variation of PCF design parameters $d/\Lambda$ and $\Lambda$ along the propagation distance $z$, and (b) variation of GVD $\beta_2(z)$ and nonlinearity $\gamma(z)$ as a function of propagation distance $z$.

a few pulse compression studies in dispersion increasing nonlinear media, they are yet to be explored. Thus, these physical conditions result in various optical media which, in turn, open several avenues for generating the high-quality self-similar USPs. In this paper, we impress the dispersion decreasing and nonlinearity increasing profiles onto the PCF by suitably varying the design parameters for compressing the chirped self-similar solitary pulses at 1550 nm. The detailed pulse compression studies in the remaining optical media will be addressed in future publications.

## 5 Self-Similar Pulse Compression

We next analyze the compression of chirped self-similar solitary pulse in a TPCF, in which the dispersion decreases exponentially and nonlinearity increases exponentially. For this purpose, we consider the TPCF of length $L = 2L_D$. We determine the initial chirp $\alpha_{20}$ as $-1.302425$ THz$^2$ for a decay rate of $\sigma = 0.3$ m$^{-1}$. To investigate the pulse compression, we solve the governing Eq. (1) by means of symmetric split-step Fourier method with an initial chirped hyperbolic secant pulse of the form $\mathrm{sech}\,(t/T_0)\exp{(i\alpha_{20}t^2/2)}$. The peak power at $z = 0$ is computed with the following relation, $P_0 = \beta_{20}/(T_0^2\gamma_0)$. Figure 7 shows the compression of chirped self-similar pulse at 1550 nm. The dotted one represents the initial pulse, whereas the solid one is the compressed pulse. Figure 8 shows the exponentially decreasing GVD as
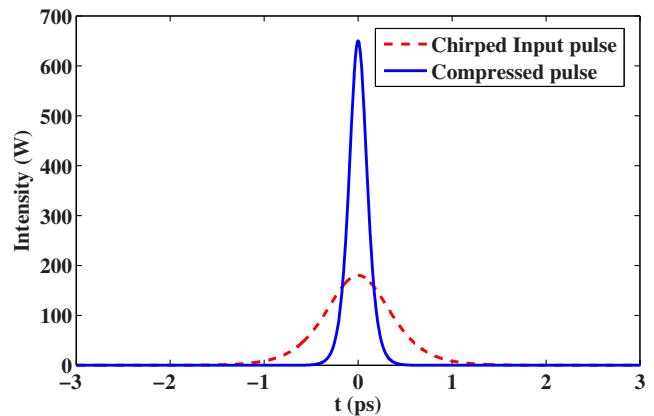


**Fig. 7** The input and output pulse of TPCF at 1550 nm. The physical parameters for self-similar scheme are $\alpha_{20} = -1.3092$ THz$^2$, $T_0 = 0.8$ ps, and $\beta_{20} = -0.0954788$ ps$^2$/m and the PCF length is $2L_D$.

the function of propagation distance $z$ for various decay rates from $\sigma = 0.01$ to $0.3$ m$^{-1}$. From this figure, it is obvious that the dispersion decay rates $\sigma = 0.25$ and $0.3$ m$^{-1}$ exhibit the exact tapering profile for maximum compression factor. However, the compression factor turns maximum (3.998) when $\sigma = 0.3$ m$^{-1}$. For a given input pulse width (FWHM) of 800 fs, the output pulse width is $\sim$201 fs. Thus, the
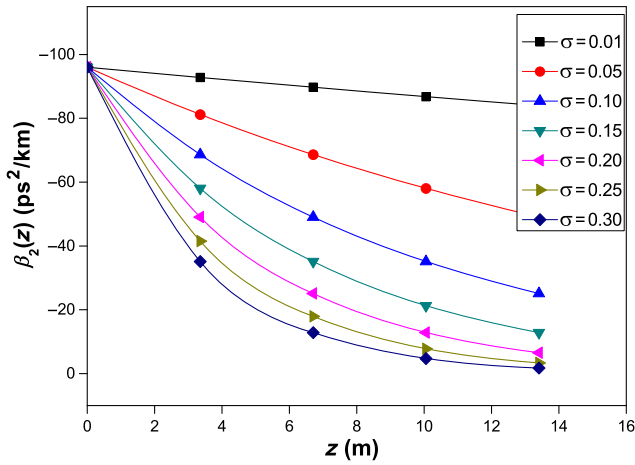
**Fig. 8** GVD decreasing profiles with decay rates from $\sigma = 0.01$ to $0.3 \text{ m}^{-1}$.



**Fig. 9** The comparison of pedestals present in the compressed pulses for the decay rates $\sigma = 0.01$ to $0.3 \text{ m}^{-1}$ along the propagation distance $z$.



**Fig. 10** Logarithmic scale of compressed pulse. Dotted line indicates initial pulse and solid line represents compressed output pulse.

compression percentage turns out to be 74.95. This in-depth analysis reveals that the exact exponentially decreasing dispersion profile plays a key role in achieving the high degree of compression.

### 5.1 Quality of Compressed Pulse

In the pulse compression process, it is of paramount importance to analyze the quality of the compressed pulses. Here, we quantify the quality of the compressed pulses based on the amount of pedestal energy generated. In general, there are a few methods to compute the pedestal energy, which include plotting of the compressed pulses in terms of logarithmic scale and by calculating the residual-field energy (RFE). The amount of pedestal energy is defined as the ratio between the total energy of the transmitted pulse and the energy of a hyperbolic secant pulse, which has the same width and peak with that of the transmitted pulse.[10] That is, pedestal energy $(\%) = (E_{\text{total}} - E_{\text{sech}})/E_{\text{total}} \times 100(\%)$, where $E_{\text{total}}$ and $E_{\text{sech}}$ are energies of the pulse at the initial and final fiber lengths. Figure 9 shows the variations of pedestal energy for various decay rates from $\sigma = 0.01$ to $0.3 \text{ m}^{-1}$. Here, the pedestal of the compressed pulse is 0.35% for $\sigma = 0.25 \text{ m}^{-1}$, whereas the decay rate ($\sigma = 0.3 \text{ m}^{-1}$), which provides the maximum compression factor, exhibits the pedestal energy around 0.38%. Thus, these two decay rates result in high-compression factors with minimal pedestals as shown in Fig. 9.

Figure 10 shows the intensity variation of the compressed pulse in terms of logarithmic scale. Here, it is obvious that the broad pedestal is seen at the bottom of the pulse, which is undesirable as it leads to intersymbol interference in fiber optic communication systems. From this figure, it may be observed that the pedestals associated with the compressed pulse are sufficiently less. Hence, they could be ignored. We can also determine this pedestal energy in terms of residual-field energy with the following expression:

$$\text{RFE}(\%) = \frac{\int_{-\infty}^{\infty} |E - E_1|^2 \text{d}t}{\int_{-\infty}^{\infty} |E|^2 \text{d}t} \times 100\%, \qquad (12)$$

where $E$ is the electric-field envelope calculated by solving the NLS equation using the split-step Fourier method and $E_1$ is the best fit of the hyperbolic secant pulse obtained
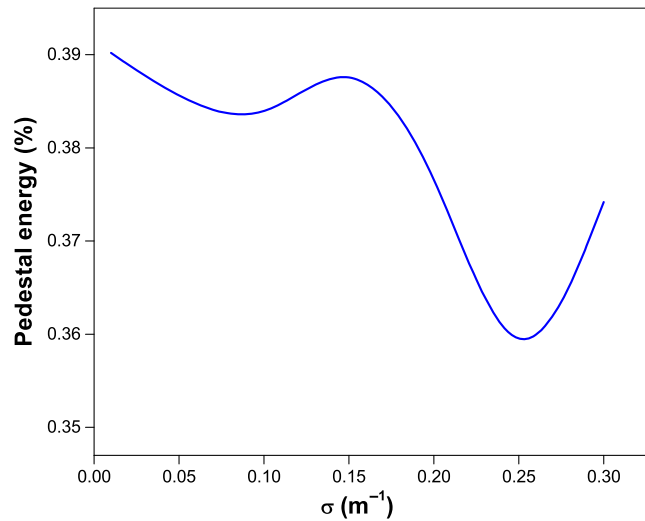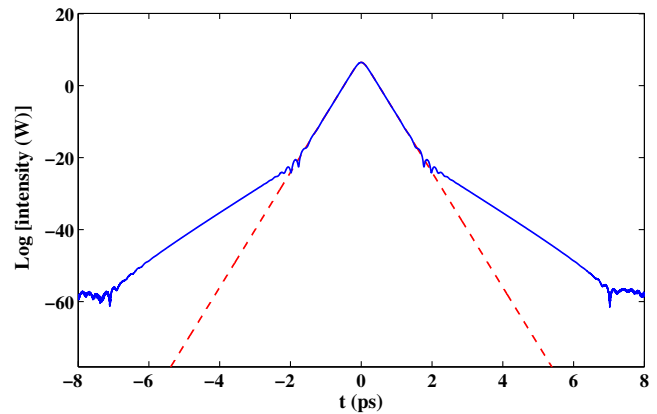
by least-mean-square fit for all the six parameters (amplitude, pulse peak temporal position, pulse width, chirp, velocity, and constant phase).[23]

Figure 11 shows the RFE evolution during the self-similar pulse compression process. Furthermore, this figure again confirms that the pedestal energy generated during the compression process is highly negligible. Therefore, it turns out that, using the proposed compressor, it is possible to generate high-quality USPs, which may not be possible with the conventional compressors.

## 6 Importance of Initial Chirp for Efficient Pulse Compression

It is well established that the linear chirp associated with the bright solitary pulse is an important requirement as it facilitates the effective pulse compression. From the analytical results, it is obvious that the dispersion decay rate depends on the initial chirp as well as the initial dispersion. It is known that, for ideal compression, the pulse should exhibit linear chirp associated with GVD and the same can be computed using the following relation $\alpha_{20} = \sigma/2\beta_{20}$.
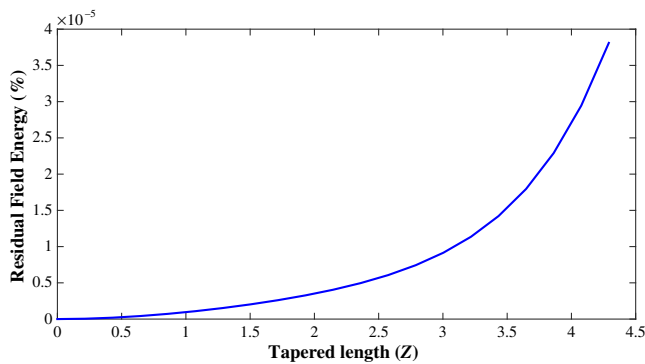
**Fig. 11** RFE evolution during the self-similar pulse compression process. The physical parameters are $\alpha_{20} = -1.3092$ THz$^2$, $T_0 = 0.8$ ps, and $\beta_{20} = -0.0954788$ ps$^2$/m and the PCF length is $2L_D$ and $\sigma = 0.3$ m$^{-1}$.

Therefore, it is essential to analyze the role of initial chirp over the compression process. Since the generation of desired hyperbolic secant pulse profile and the prescribed chirp is highly challenging, the compression technique for pulses with an arbitrary initial chirp and shape is of practical interest. To do so, we plot exponentially decreasing GVD for various decay rates and the same is shown in Fig. 8. This analysis allows one to estimate the optimal exponentially decreasing profile for the efficient pulse compression. From the detailed pulse compression analysis, we infer that the dispersion decreasing profiles with $\sigma = 0.25$ and $0.3$ m$^{-1}$ exhibit the exact exponential decreasing nature along the propagation distance as the compression factor turns maximum and pedestal energy is minimum for these profiles, which would help achieve efficient pulse compression. Hence, we compute the initial linear chirp from the best exponential fit.

## 7 Conclusion

In this work, we have identified the four possible physically valid conditions for the existence of chirped self-similar solitary pulses in the TPCFs. Further, these physical conditions have paved the way for getting the necessary insight in having realized the different designs of PCFs capable of providing high-quality compressed pulses at 1550 nm. Having chosen the exponentially decreasing dispersion and nonlinearity increasing medium, we have explored the pulse compression studies for various decay rates from $\sigma = 0.01$ to $0.3$ m$^{-1}$. Based on the numerical results, we have inferred that the dispersion decreasing profiles with $\sigma = 0.25$ and $0.3$ m$^{-1}$ exhibit the exact exponential decreasing nature along the propagation distance as the compression factor turns maximum and pedestal energy is minimum. In addition, the quality of the compressed pulses has been addressed in terms of RFE and intensity of the compressed pulse in terms of logarithmic plot. To summarize, the ultimate crux of this work lies in having identified the appropriate variations of dispersion and nonlinearity for obtaining high-quality pulses at 1550 nm.

### References

1. G. Agrawal, *Applications of Nonlinear Fiber Optics*, Academic Press, San Diego, California (2001).
2. R. Holzwarth et al., "Optical frequency synthesizer for precision spectroscopy," *Phys. Rev. Lett.* **85**, 2264–2267 (2000).
3. J. Valdmanis and G. Mourou, "Subpicosecond electrooptic sampling: principles and applications," *IEEE J. Quantum Electron.* **22**(1), 69–78 (1986).
4. L. Fu et al., "Efficient optical pulse compression using chalcogenide single-mode fibers," *Appl. Phys. Lett.* **88**(8), 081116 (2006).
5. L. F. Mollenauer, R. H. Stolen, and J. P. Gordon, "Experimental observation of picosecond pulse narrowing and solitons in optical fibers," *Phys. Rev. Lett.* **45**, 1095–1098 (1980).
6. K. C. Chan and H. F. Liu, "Short pulse generation by higher order soliton-effect compression: effects of optical fiber characteristics," *IEEE J. Quantum Electron.* **31**(12), 2226–2235 (1995).
7. S. Smirnov et al., "Optical spectral broadening and supercontinuum generation in telecom applications," *Opt. Fiber Tech.* **12**(2), 122–147 (2006).
8. M. Pelusi and H.-F. Liu, "Higher order soliton pulse compression in dispersion-decreasing optical fibers," *IEEE J. Quantum Electron.* **33**(8), 1430–1439 (1997).
9. J. D. Moores, "Nonlinear compression of chirped solitary waves with and without phase modulation," *Opt. Lett.* **21**, 555–557 (1996).
10. K. Senthilnathan et al., "Robust pedestal-free pulse compression in cubic-quintic nonlinear media," *Phys. Rev. A* **78**(3), 033835 (2008).
11. Q. Li et al., "Nearly chirp- and pedestal-free pulse compression in nonlinear fiber Bragg gratings," *J. Opt. Soc. Am. B* **26**, 432–443 (2009).
12. R. Black et al., "Tapered single-mode fibres and devices. II. Experimental and theoretical quantification," *IEE Proc. J. Optoelectron.* **138**(5), 355–364 (1991).
13. K. Saitoh and M. Koshiba, "Full-vectorial imaginary-distance beam propagation method based on a finite element scheme: application to photonic crystal fibers," *IEEE J. Quantum Electron.* **38**(7), 927–933 (2002).
14. S. Varshney et al., "Design and simulation of 1310 nm and 1480 nm single-mode photonic crystal fiber Raman lasers," *Opt. Express* **16**, 549–559 (2008).
15. T. A. Birks and Y. W. Li, "The shape of fiber tapers," *J. Lightwave Technol.* **10**(4), 432–438 (1992).
16. F. Bilodeau et al., "Low-loss highly overcoupled fused couplers: fabrication and sensitivity to external pressure," *J. Lightwave Technol.* **6**(10), 1476–1482 (1988).
17. J. Dewynne, J. Ockendon, and P. Wilmott, "On a mathematical model for fiber tapering," *SIAM J. Appl. Math.* **49**(4), 983–990 (1989).
18. M. Eisenmann and E. Weidel, "Single-mode fused biconical couplers for wavelength division multiplexing with channel spacing between 100 and 300 nm," *J. Lightwave Technol.* **6**(1), 113–119 (1988).
19. G. Humbert et al., "Supercontinuum generation system for optical coherence tomography based on tapered photonic crystal fibre," *Opt. Express* **14**, 1596–1603 (2006).
20. S. Roy, K. Mondal, and P. R. Chaudhuri, "Modeling the tapering effects of fabricated photonic crystal fibers and tailoring birefringence, dispersion, and supercontinuum generation properties," *Appl. Opt.* **48**, G106–G113 (2009).
21. J. Hu et al., "Pulse compression using a tapered microstructure optical fiber," *Opt. Express* **14**, 4026–4036 (2006).
22. J. C. Travers et al., "Optical pulse compression in dispersion decreasing photonic crystal fiber," *Opt. Express* **15**, 13203–13211 (2007).
23. R. Zhang, J. Teipel, and H. Giessen, "Theoretical design of a liquid-core photonic crystal fiber for supercontinuum generation," *Opt. Express* **14**, 6800–6812 (2006).
24. Comsol Multiphysics v. 3.5a (2008).
25. W. J. Wadsworth et al., "Supercontinuum generation in photonic crystal fibers and optical fiber tapers: a novel light source," *J. Opt. Soc. Am. B* **19**, 2148–2155 (2002).
26. J. Cascante-Vindas et al., "White light supercontinuum generation in a Y-shaped microstructured tapered fiber pumped at 1064 nm," *Opt. Express* **18**, 14535–14540 (2010).
27. H. W. Chen et al., "Visible supercontinuum generation in tapered photonic crystal fiber pumped by picosecond pulse at 1064 nm," *Laser Phys.* **22**(8), 1321–1324 (2012).

**Annamalai Manimegalai** received her BE degree in electronics and communication engineering from the University of Madras, India. She received her ME degree in applied electronics from Anna University, India. Currently, she is working as a professor in the Department of ECE, Ganadipathy Tulsi's Jain Engineering College, Vellore, as well as pursuing her PhD at VIT University, Vellore. She is a member of IEEE, and a life member of IETE and the Indian Society for Technical Education.

**Krishnamoorthy Senthilnathan** received his MSc and MPhil degrees in physics from the University of Madras, India. He received

his PhD from Anna University, India. He worked as postdoctoral fellow in Hong Kong Polytechnic University. Later, he joined as an assistant professor at NIT, Rourkela. Currently, he is working as an associate professor in the Department of Physics, VIT University, Vellore, India. His primary research interests include modeling the photonic devices using photonic crystal fibers.

**Kaliyaperumal Nakkeeran** received his PhD from Anna University, Chennai, India, in 1998. From 1999 to 2005, he was a postdoc at three different institutes, the Institute of Mathematical Sciences, Chennai, India, University of Burgundy, Dijon, France, and the Hong Kong Polytechnic University, Hong Kong. Since 2005, he has been a senior lecturer with the School of Engineering, University of Aberdeen, Aberdeen, United Kingdom. His research interests include modeling and simulations of nonlinear optical fiber systems.

**Padmanabhan Ramesh Babu** received his MSc, MPhil, and PhD degrees in physics from the University of Madras, India. Currently, he is working as a professor in the Department of Physics, VIT University, Vellore, India. His research interests include photonic crystal fibers, Bragg gratings, and optical fiber communications. He is a life member of Indian Association of Physics Teachers, Indian Society for Technical Education as well as Indian Laser Association.